Rugate filter for light-trapping in solar cells

Stephan Fahr,[1] **Carolin Ulbrich,**[2] **Thomas Kirchartz,**[3] **Uwe Rau,**[3]
Carsten Rockstuhl,[1] **and Falk Lederer,**[1]

[1]*Institut für Festkörpertheorie und -optik, Max-Wien-Platz 1, 07743, Jena, Germany*
[2]*Institut für Physikalische Elektronik, Pfaffenwaldring 47, 70569, Stuttgart, Germany*
[3]*IEF-5 Photovoltaik, Forschungszentrum Jülich, 52425, Jülich, Germany*

stephan.fahr@uni-jena.de

Abstract: We suggest a design for a coating that could be applied on top
of any solar cell having at least one diffusing surface. This coating acts as
an angle and wavelength selective filter, which increases the average path
length and absorptance at long wavelengths without altering the solar cell
performance at short wavelengths. The filter design is based on a continuous
variation of the refractive index in order to minimize undesired reflection
losses. Numerical procedures are used to optimize the filter for a $10\,\mu m$
thick monocrystalline silicon solar cell, which lifts the efficiency above the
Auger limit for unconcentrated illumination. The feasibility to fabricate such
filters is also discussed, considering a finite available refractive index range.

© 2008 Optical Society of America

OCIS codes: (040.5350) Photovoltaic; (220.1770) Concentrators; (230.4170) Multilayers;
(310.0310) Thin films; (350.2460) Filters, interference; (350.6050) Solar energy.

References and links

1. W. Shockley and H. J. Queisser, "Detailed Balance Limit of Efficiency of p-n Junction Solar Cells," J. Appl. Phys. **32**, 510–519 (1961).
2. M. J. Kerr, A. Cuevas, and P. Campbell, "Limiting Efficiency of Crystalline Silicon Solar Cells Due to Coulomb-Enhanced Auger Recombination," Prog. Photovoltaics **11**, 97–104 (2002).
3. D. Redfield, "Multiple-pass thin-film silicon solar cell," Appl. Phys. Lett. **25**, 647–648 (1974).
4. E. Yablonovitch, "Statistical ray optics," J. Opt. Soc. Am. **72**, 899–907 (1982).
5. M. A. Green, "Lambertian light trapping in textured solar cells and light-emitting diodes: analytical solutions," Prog. Photovoltaics **10**, 235–241 (2002).
6. P. Bermel, C. Luo, L. Zeng, L. C. Kimerling, and J. D. Joannopoulos, "Improving thin-film crystalline silicon solar cell efficiencies with photonic crystals," Opt. Express **15**, 16986–17000 (2007).
7. L. Zeng, Y. Yi, C. Hong, J. Liu, N. Feng, X. Duan, L. C. Kimerling, and B. A. Alamariu, "Efficiency enhancement in Si solar cells by textured photonic crystal back reflector," Appl. Phys. Lett. **89**, 111111 (2006).
8. P. Campbell, "Enhancement of light absorption from randomizing and geometric textures," J. Opt. Soc. Am. B **10**, 2410–2415 (1993).
9. P. Campbell and M. A. Green, "Light trapping properties of pyramidally textured surfaces," J. Appl. Phys. **62**, 243–249 (1987).
10. S. Fahr, C. Rockstuhl, and F. Lederer, "Engineering the randomness for enhanced absorption in solar cells," Appl. Phys. Lett. **92**, 171114 (2008).
11. C. Rockstuhl, F. Lederer, K. Bittkau, and R. Carius, "Light localization at randomly textured surfaces for solar-cell applications," Appl. Phys. Lett. **91**, 1104–1106 (2007).
12. J. C. Miñano, *Physical Limitations to Photovoltaic Energy Conversion*, chap. Optical confinement in photovoltaics, pp. 50–83 (Adam Hilger, Bristol, 1990).
13. D. Buie and A. G. Monger, "The effect of circumsolar radiation on a solar concentrating system," Sol. energy **76**, 181–185 (2004).
14. C. Ulbrich, S. Fahr, M. Peters, J. Üpping, T. Kirchartz, C. Rockstuhl, J. C. Goldschmidt, P. Löper, R. Wehrspohn, A. Gombert, F. Lederer, and U. Rau, "Directional selectivity and light-trapping in solar cells," Photonics for Solar Energy Systems II **7002**, 70020A (2008).

15. J. A. Dobrowolski and D. G. Lowe, "Optical thin film synthesis program based on the use of Fourier transforms," Appl. Opt. **17**, 3039–3050 (1978).
16. P. Baumeister, "Design of multilayer filters by successive approximations," J. Opt. Soc. Am. (1917-1983) **48**, 955–958 (1958).
17. P. G. Verly, A. V. Tikhonravov, and M. K. Trubetskov, "Efficient refinement algorithm for the synthesis of inhomogeneous optical coatings," Appl. Opt. **36**, 1487–1495 (1997).
18. J.-M. Yang and C.-Y. Kao, "An Evolutionary Algorithm for the Synthesis of Multilayer Coatings at Oblique Light Incidence," J. Lightwave Technol. **19**, 559–570 (2001).
19. S. Kirkpatrick, J. Gelatt, C. D., and M. P. Vecchi, "Optimization by Simulated Annealing," Science **220**, 671–680 (1983).
20. M. F. Schubert, F. W. Mont, S. Chhajed, D. J. Poxson, J. K. Kim, and E. F. Schubert, "Design of multilayer antireflection coatings made from co-sputtered and low-refractive-index materials by genetic algorithm," Opt. Express **16**, 5290–5298 (2008).
21. W. H. Southwell, "Gradient-index antireflection coatings," Opt. Lett. **8**, 584–586 (1983).
22. R. Jacobsson, "Inhomogeneous and coevaporated homogeneous films for optical applications," Phys. Thin Films **8**, 51–98 (1975).
23. E. Lorenzo, C. J. Oton, N. E. Capuj, M. Ghulinyan, D. Navarro-Urrios, Z. Gaburro, and L. Pavesi, "Porous silicon-based rugate filters," Appl. Opt. **44**, 5415–5421 (2005).
24. G. Boivin and D. St.-Germain, "Synthesis of gradient-index profiles corresponding to spectral reflectance derived by inverse Fourier transform," Appl. Opt. **26**, 4209–4213 (1987).
25. B. G. Bovard, "Rugate filter theory: an overview," Appl. Opt. **32**, 5427–5442 (1993).
26. W. H. Southwell, "Extended-bandwidth reflector designs by using wavelets," Appl. Opt. **36**, 314–318 (1997).
27. W. Southwell, "Using apodization functions to reduce sidelobes in rugate filters," Appl. Opt. **28**, 5091–5094 (1989).
28. M. J. Minot, "The angular reflectance of single-layer gradient refractive-index films," J. Opt. Soc. Am. **67**, 1046–1050 (1977).
29. W. Southwell, "Omnidirectional Mirror Design With Quarter-Wave Dielectric Stacks," Appl. Opt. **38**, 5464–5467 (1999).
30. P. A. Basore and D. A. Clugston, "PC1D Version 5.1" (1997).
31. M. J. Kerr and A. Cuevas, "General parameterization of Auger recombination in crystalline silicon," J. Appl. Phys. **91**, 2473–2480 (2002).
32. J. A. Nelder and R. Mead, "A Simplex Method for Function Minimization," Comput. J. **7**, 308–313 (1965).
33. J. Q. Xi, M. F. Schubert, J. K. Kim, E. F. Schubert, M. Chen, S.-Y. Lin, W. Liu, and J. A. Smart, "Optical thin-film materials with low refractive index for broadband elimination of Fresnel reflection," Nat. Photon. **1**, 176–179 (2007).
34. W. J. Gunning, R. L. Hall, F. J. Woodberry, W. H. Southwell, and N. S. Gluck, "Codeposition of continuous composition rugate filters," Appl. Opt. **28**, 2945–2948 (1989).

1. Introduction

Reduced recombination current, less material consumption, and better carrier collection are the fundamental intentions for making thinner solar cells. In order to maintain a sufficient light absorption, the incoming light has to be efficiently trapped. This is particularly important when the absorbing material is an indirect semiconductor. For these materials, such as silicon (Si), a limit for the photovoltaic conversion efficiency η based on the absorption was found at first by Shockley and Queisser. Assuming each absorbed photon generates one electron-hole-pair, they showed that the efficiency limit is 31% [1], as long as no nonradiative losses are included. Kerr *et al.* [2] found recently a more realistic limit of approximately 28% for Si by including Coulomb-enhanced Auger recombination processes and other realistic silicon-specific processes for unconcentrated illumination.

Enhancing the absorption by an appropriate light-trapping scheme would result in an increased short circuit current density J_{SC}. This implies that the cells could be made with a thinner Si layer and would still provide the same J_{SC}. In such a configuration, the advantage is a lower bulk recombination that leads to a higher open circuit voltage V_{OC}. Either a larger J_{SC} or V_{OC} will enhance η.

The term light-trapping refers to the redistribution of the incoming light into new directions within the solar cell. Ideally, total internal reflection will then prevent this redirected light from

escaping the solar cell [3]. A perfect back side reflector and a Lambertian (isotropic) distribution of light inside the solar cell will increase the percentage of light that is trapped by total internal reflection. The path length enhancement k is usually regarded as a measure for the light-trapping. The combination of the back side reflector and the Lambertian light distribution leads to an effective path length enhancement of $k = 4n^2$ [4,5], with n being the refractive index of the solar cell material. In the case of a standard semiconductor solar cell ($n = 3.5$) $k \approx 50$ may be achieved. Note that an absorption enhancement can also be obtained by applying other photonic concepts, such as periodically structured back reflectors, which are optimized to increase the optical path length for wavelengths around the band gap of the absorbing layer [6, 7]. The Lambertian light distribution is generally attained by incorporating an appropriately structured surface [8, 9, 10, 11], whose nature can be either statistical (rough surfaces) or deterministic (e.g. periodic arrangement). For unconcentrated illumination the solar cell absorbs light incident from all directions, i.e. the acceptance cone of a device as described above is assumed to be the entire half-space above the solar cell.

Ultra light-trapping relates to a restriction of the acceptance cone of the solar cell in combination with a tracking system, which ensures normal incidence of the direct sun light all the time. Applying an angle selective filter, which restricts the acceptance cone, on top of a solar cell having at least one Lambertian surface, will enlarge k up to $4n^2/\sin^2\theta$ [12]. Here θ depicts the opening angle of the restricted acceptance cone. The aperture of the circumsolar disc, being approximately $5°$ [13], corresponds to the smallest acceptance cone that can be reasonably chosen, as all circumsolar light shall still enter the solar cell. This limitation permits an enhancement of k up to ~ 6450. Using such a minimal acceptance cone comes at the expense of a tracking system for the solar cell.
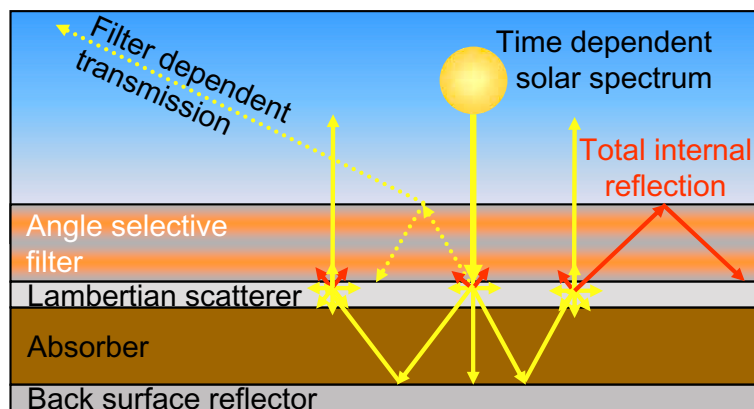

Fig. 1. Schematic drawing of the solar cell considered throughout this paper.

Figure 1 shows a schematic drawing of the solar cell considered in this paper. From top to bottom this solar cells consists of an angle- and wavelength selective filter, a perfect Lambertian scatterer, an absorbing layer, and a perfect back reflector. The direct sunlight impinges normally onto the solar cell, passes the angle selective filter, and is scattered isotropically by the diffusor. The Lambertian scatterer was assumed to be impedance matched to the following absorbing layer and, therefore, does not cause additional reflections at the diffusor-absorber interface. Electron hole pairs are generated inside the absorbing layer, which was exemplarily chosen to be a 10 µm thick monocrystalline Si layer. Outgoing solar cell radiation, consisting of reemitted and not-absorbed light, which passed already through the Lambertian scatterer, is trapped inside the cell according to the angle and wavelength dependent filter reflectance.

At first glance, limiting the acceptance cone to the aperture of the circumsolar disc independent of the wavelengths, should lead to the highest possible efficiency. Since terrestrial solar cells are exposed to a significant fraction of diffuse light, the limitation of the acceptance cone is desirable only in the spectral domain of weak absorption close to the band gap [14]. Figure 2 shows the ideal filter transmission as a function of wavelength and angle of incidence, which is measured relative to the surface normal throughout this paper. The ideal filter shows *perfect transmission* up to a wavelength of $\sim 870\,\text{nm}$. For longer wavelengths up to $\sim 1300\,\text{nm}$ the filter should be *perfectly reflecting* only for angles of incidence larger than $2.5\,°$. The optical characteristics of the filter above $\sim 1300\,\text{nm}$ will not affect η, as the energy of the light is too small to permit for an absorption by Si. The exact threshold wavelength of the transition between *perfect transmission* and *perfect reflection* depends on the thickness, the wavelength dependent absorption coefficient, and the spectra of the direct sunlight and of the diffuse scattered light from the sky. For the $10\,\mu\text{m}$ thick monocrystalline Si-layer considered in this paper, the threshold wavelength was determined to be around $870\,\text{nm}$ [14].
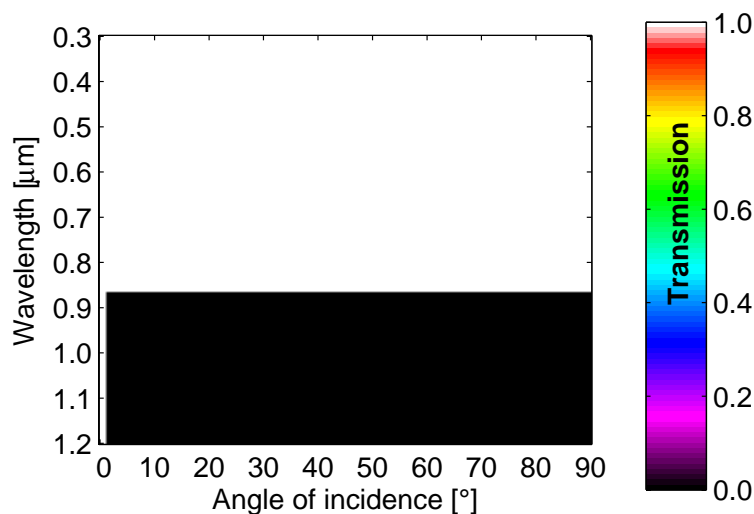

Fig. 2. Transmission of unpolarized light of the ideal wavelength and angle selective filter considered in this paper.

It is the aim of this paper to present a design for a realizable filter that approximates this ideal filter function for the, to a certain extend arbitrarily, selected solar cell. This filter can be applied to the top of any solar cell having at least one diffusing surface, where it will decrease the acceptance cone. The filter is based on an appropriately designed and optimized sequence of dielectric layers. In order to be as general as possible we did not restrict the coating materials from the beginning, hence dispersion and absorption of the coating are neglected throughout this paper. Upon evaluating the impact of the filter on the solar cells efficiency it will be shown that values for the efficiency above the 28% limit predicted by Kerr *et al.* [2] can be reached. After outlining the principles for the filter design, the design of the coating system is described in detail. Finally, the filter is numerically optimized by adopting the filter onto a solar cell in a simulation allowing to calculate the efficiency, which is used as the measure to be optimized.

2. Coating design

Various methods for the design of optical coatings have been developed. All of them have certain advantages but also some intrinsic disadvantages. Synthesis methods [15] employ physical

understanding of already known solutions for creating an initial refractive index profile. Refinement methods [16, 17], in turn, require an initial layer stack design and can then minimize a merit function by adjusting coating parameters, for example the thickness and the corresponding refractive index. In cases, where either the problem is too complicated or where such initial solutions do not exist, global optimization techniques are commonly used. Examples for such techniques are genetic algorithms [18] or simulated annealing [19]. Such methods are able to find an, at least local, optimum. However, currently it is too time consuming to check the entire parameter space, thus these methods generally lack proof that their final solutions are among the best. Furthermore, one obtains no insight into the underlying physics on that the filter relies or why these particular solutions are superior to others.

In this paper, we derive a design for a filter from already known ingredients. The design process is divided into four steps. At first, the perfect anti-reflection-(AR)-property of the coating is realized. At second, the implementation of a single reflection band is demonstrated. Third, the side lobes due to the finiteness of the coating system are suppressed. The presence of such side lobes would seriously degrade the overall performance of the cell. Finally, all design steps are combined and a final refinement procedure is applied to optimize the filter function for a given solar cell.

2.1. Perfect transmission

At an interface, which separates two media having different refractive indices n_1 and n_2, Fresnel reflection occurs. The simplest AR-coating is a single quarter wave layer with an index of refraction of $\sqrt{n_1 n_2}$. However, this single layer permits perfect AR only at the design wavelength, although additional layers can be used to broaden the AR-wavelength region [20].

Southwell proposed a continuous profile of the refractive index [21] instead of using discrete indices of refraction. In order to express analytical refractive index profiles we define the z-axis to be normal to the interface. The spatial position of the interface between the two media is set to be at $z = 0$. Since transmission and reflection coefficients of layer systems depend only on phase differences, the optical thickness t (defined by $t = \int n(z)\mathrm{d}z$ and $t = 0$ at the interface) becomes the argument of refractive index profiles $n(t)$. The proposed profile is a quintic polynomial given by

$$n(t_\mathrm{n}) = n_1 + (n_2 - n_1)(6t_\mathrm{n}^5 - 15t_\mathrm{n}^4 + 10t_\mathrm{n}^3), \tag{1}$$

where t_n is the optical thickness normalized to the total optical thickness, thus taking values between 0 and 1. Figure 3(a) shows the profile and Fig. 3(b) the broadband AR-behavior for a 1 μm thick coating. The transmission calculations were performed by applying the matrix method [22]. As can be seen, nearly perfect transmission for all angles of incidence and both polarizations occurs for a ratio between the wavelength and the total optical thickness smaller than ~ 1.0. It should be noted that a quintic profile is not optimum [21], but its simple analytical description makes it favorable.

2.2. Perfect reflection

A second issue, besides perfect transmission over a large spectral range, is a perfect reflection over a narrow spectral domain. Figure 4 shows the refractive index profiles and the corresponding reflection as a function of the wavelength for three possible filters which show perfect reflection in a certain wavelength range. The design wavelength for perfect reflection was chosen to be $\lambda_0 = 1.0$ μm for all profiles.

The simplest filter function is made using a binary quarter-wave-stack, i.e. a sequence of layers of alternating high (n_max) and low (n_min) refractive indices with optical thicknesses equal to a quarter wavelength. Unfortunately, the binary elements give rise to other reflection peaks at odd multiples of the fundamental wave number [see the dotted line in Fig. 4(b) around 0.33 μm].
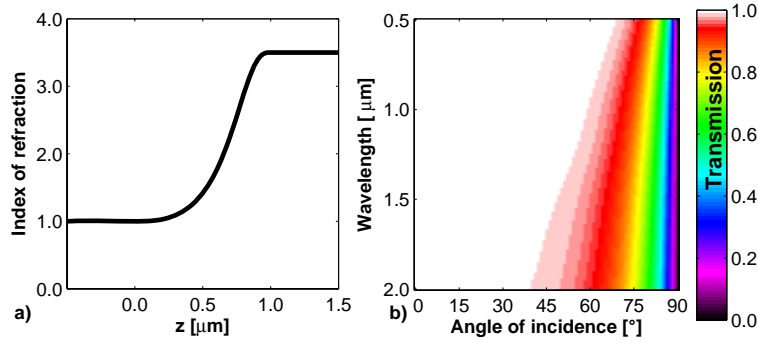
Fig. 3. a) A 1 µm thick quintic continuous refractive index profile going from 1.0 to 3.5. b) The corresponding angle and wavelength dependent transmission of unpolarized light. The structure shows nearly perfect transmission for wavelength to AR-coating thickness ratios smaller than 1.0. The white region corresponds to more than 99% transmission.
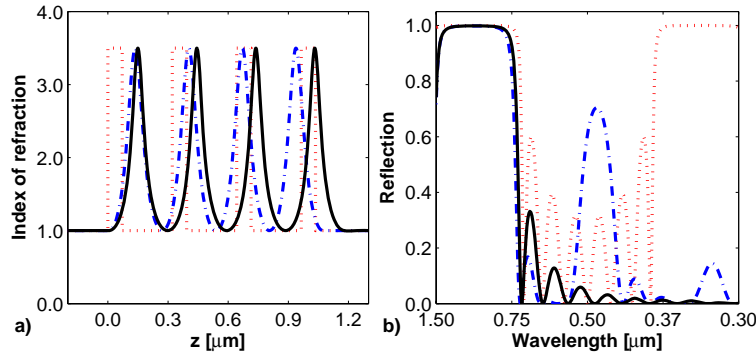

Fig. 4. a) Four periods of a binary (dotted), a sinusoidal (dash-dot) and an exponential sinusoidal (solid) refractive index profile for $n_{\min} = 1.0$ and $n_{\max} = 3.5$ at a design wavelength of $\lambda_0 = 1.0$ µm. b) The corresponding wavelength dependent reflection of each filter.

It is well known that sinusoidal profiles, given by

$$n(t) = n_{\min} + \frac{n_{\max} - n_{\min}}{2} \left[1 + \sin\left(\frac{4\pi}{\lambda_0}t - \frac{\pi}{2}\right)\right], \tag{2}$$

exhibit weaker reflection peaks at higher orders [23]. But they have the drawback, that reflection peaks appear in the reflection curve also at even multiples of the fundamental wave number [see the dash-dotted line in Fig. 4(b) at 0.50 µm]. Nevertheless, as is shown, these higher reflection bands are less pronounced.

When applying the Fourier synthesis method [24, 25] further suppression of higher order reflection bands is achieved. This is possible by choosing an exponential profile with a sinusoidal argument [23, 26], like

$$n(t) = \sqrt{n_{\min}n_{\max}} \exp\left[\frac{\ln(\frac{n_{\max}}{n_{\min}})}{2} \sin\left(\frac{4\pi}{\lambda_0}t - \frac{\pi}{2}\right)\right]. \tag{3}$$

Only a single reflection band around λ_0 is observed for this profile; thus, this is the preferable geometry.

2.3. Side lobe elimination

The remaining oscillations in the reflection spectrum of the exponential sinusoidal profile are due to the limited number of periods taken into account. Therefore, they can be associated with Fabry-Perot-oscillations, due to the sharply truncated refractive index profile. In order to avoid these side lobes [27] special window functions (Hartman, Kaiser, Gauss etc.) have been established in signal processing areas. In summary, an exponential sinusoidal refractive index profile together with a smooth envelope function [see Fig. 5(a)] will give rise to a single reflection band around λ_0. In the remaining wavelength domain complete transmission is observed [see Fig. 5(b) at normal incidence].
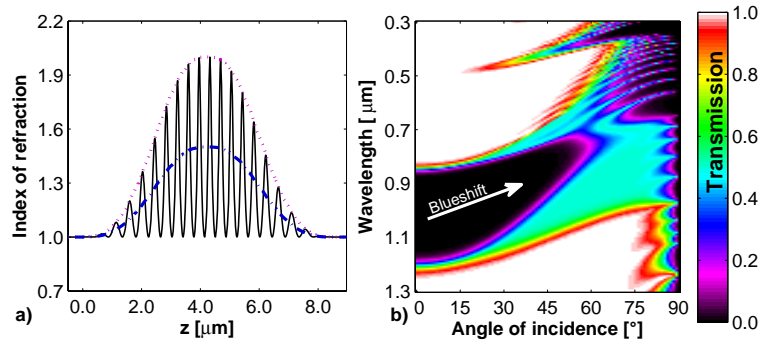

Fig. 5. a) Exponential sinusoidal refractive index profile (solid line) with quintic amplitude function (dotted line). The dash-dotted line represents the averaged refractive index. b) The angle resolved transmission spectrum shows the desired blue shift of the stop band when tilting the angle of incidence.

The continuous nature of the averaged refractive index (dash-dotted line in Fig.5(a)) allows for a less polarization dependent AR-coating at tilted angles of incidence as compared to discrete layer systems [28], which is mandatory for the applicability in photovoltaic systems.

2.4. Reflection at oblique incidence

The well known blue shift [29] of a reflection band when tilting the angle of incidence can be clearly seen in the angle resolved reflection spectrum shown in Fig. 5(b) for the structure presented in Fig. 5(a).

At short wavelengths a broad area with AR properties can be identified, which will allow the light scattered from the sky to enter the solar cell. Furthermore, the blue shift leads to the desired high reflection for tilted angles, but only for the wavelength region between 700 and 800 nm. Scaling the thickness of the layer system will shift the position of the stop band. Due to reciprocity, this high reflectivity at oblique incidence will also appear for light hitting the surface from inside the solar cell. Thus the escape cone will be limited further. This will allow for longer absorption path lengths in the long wavelength region.

In the following section we optimize the parameters, which describe the profile of the index of refraction, to increase η due to light-trapping.

3. Parameter optimization

So far, we presented refractive index profiles leading to a perfect AR-coating (see Fig. 3) and to the desired angle-selectivity (see Fig. 5). The combination of these elements leads to the dependence of the refractive index profile on the optical thickness as depicted in Fig. 6. The

entire profile can be described with only a few parameters. The first one is the total optical thickness (t_{tot}) of the entire coating system. The second is the position of the stop band (λ_0). Reflection losses are minimized by quintic matching of the average refractive index (dotted line in Fig. 6) in regions I (front) and III (back). Side lobes are suppressed by using smooth (quintic) envelope functions (dash-dotted lines in Fig. 6) in these regions, too. The optical thickness of these regions is, therefore, also a parameter and is denoted by t_{apo}. It was found that the phase of the sinusoidal function does not have a large influence, i.e. it is not necessary to find an optimum value.
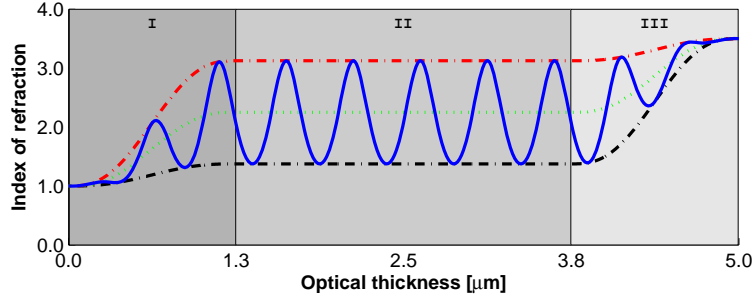

Fig. 6. Refractive index profile versus *optical* thickness for $t_{tot} = 5$ μm, $\lambda_0 = 1$ μm, $t_{apo} = 0.25 \times t_{tot}$, $A_{max} = 0.7$, $n_{inc} = 1.0$, and $n_{sub} = 3.5$.

For the first optimization we introduce an additional parameter A_{max}, which represents the maximum amplitude of the refractive index modulation. The indices of refraction of the incidence medium and the subsequent solar cell are represented in the following by n_{inc} and n_{sub}, respectively. When looking at Eq. (3), it is clear that the magnitudes for the minimum and maximum indices of refraction are needed. They are represented by n_{min} and n_{max}, respectively. In region II ($t_{apo} < t_{II} < t_{tot} - t_{apo}$), where n_{min} and n_{max} are constant, they are given by

$$n_{min,II} = \frac{n_{sub} + n_{inc}}{2} - A_{max}\frac{n_{sub} - n_{inc}}{2} \tag{4}$$

$$n_{max,II} = \frac{n_{sub} + n_{inc}}{2} + A_{max}\frac{n_{sub} - n_{inc}}{2}, \tag{5}$$

respectively. In region I ($0 < t_I < t_{apo}$), n_{min} and n_{max} read as:

$$n_{min,I}(t_{n,I}) = n_{inc} + (n_{min,II} - n_{inc})Q(t_{n,I}) \tag{6}$$

$$n_{max,I}(t_{n,I}) = n_{inc} + (n_{max,II} - n_{inc})Q(t_{n,I}), \tag{7}$$

where

$$Q(x) = (6x^5 - 15x^4 + 10x^3) \tag{8}$$

and $t_{n,I}$ is the normalized optical thickness, which amounts to 1, when $t = t_{apo}$. In region III ($t_{tot} - t_{apo} < t_{III} < t_{tot}$) they are given by:

$$n_{min,III}(t_{n,III}) = n_{min,II} + (n_{sub} - n_{min,II})Q(t_{n,III}) \tag{9}$$

$$n_{max,III}(t_{n,III}) = n_{max,II} + (n_{sub} - n_{max,II})Q(t_{n,III}), \tag{10}$$

where $t_{n,III}$ is proportional to the optical thickness, so that $t_{n,III} = 0$, if $t = t_{tot} - t_{apo}$ and $t_{n,III} = 1$, if $t = t_{tot}$. Figure 6 shows the refractive index profile versus the *optical* thickness for $t_{tot} = 5$ μm, $\lambda_0 = 1$ μm, $t_{apo} = 0.25 \times t_{tot}$, $A_{max} = 0.7$, $n_{inc} = 1.0$, and $n_{sub} = 3.5$. The refractive indices n_{inc} and n_{sub} remain fixed in all further considerations.

To evaluate the filter performance on the solar cell efficiency, we used an algorithm described in Ref. [14], which allows the computation of η. This algorithm takes into account the position of the sun, the angle between the normal of the solar cell and the sun, and the time dependent solar spectrum. A schematic drawing of the evaluated solar cell is shown in Fig. 1. The absorber was a 10 μm thick monocrystalline Si layer, whose absorption coefficient was taken from literature [30]. The absorption inside the solar cell was then calculated following the method for a cell with Lambertian scatterer and a perfect back side reflector [5]. We assumed a cell dopant concentration of 1.5×10^{16} cm^{-3}, the back side recombination velocity was set to zero, and Auger recombination processes were included according to Ref. [31]. The calculated efficiencies represent the accumulated converted amount of energy which impinges during a standard day in Stuttgart, Germany, when the solar cell constantly faces the sun by using a tracking system.

The reference value was calculated for a solar cell with a perfect AR coating, e.g. light from all directions, at all wavelengths and polarizations, completely penetrates the filter. Such a perfect AR-filter leads to the reference efficiency of 28.7%. We performed 1000 Simplex optimization routines [32] on random starting parameters. The free parameters, which should be optimized, are: t_{tot}, λ_0, $\frac{t_{apo}}{t_{tot}}$, and A_{max}. The coating refractive indices were allowed to take all values between 1.0 and 3.5. The best among these 1000 optima is shown in Fig. 7. An η of 30.1% is achieved, i.e. an increase of 1.4 absolute %. The parameters are listed in Tab. 1.
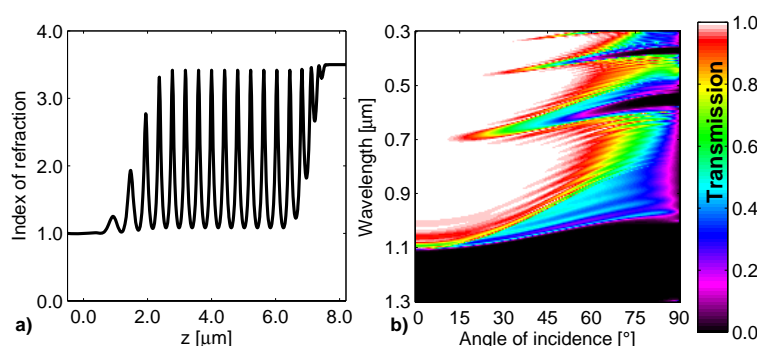

Fig. 7. a) Optimized refractive index profile, values were allowed to lie between 1.0 and 3.5. b) Angle resolved transmission spectrum leads to an efficiency of 30.1%.

4. Producibility of such filters

The presented design requires indices of refraction close to 1 to obtain the perfect AR property. With porous silicon [23] indices of refraction close to air and up to silicon are possible. Using only silicon would simplify the fabrication, as it would permit a monolithic integration, unfortunately the high absorption coefficient in the short wavelength range prohibits its use. It was shown recently that oblique angle deposition of SiO_2 can be used to provide indices of refraction as close to air as 1.05 [33]. Values up to 2.5 are possible with TiO_2, too. The gap between 2.5 and silicon would lead to some remaining back reflection that is undesirable. However, since the value of 2.5 is already high, we expect the back reflection to be only in the order of 4%.

When taking into account the stability of the coating system, fabrication by co-deposition [34] seems more reasonable. This method also allows for a continuous modulation of the refractive index, but only between those of the two materials involved.

Figure 8 (a) shows the refractive index profile of a quintic AR-coating given by Eq. (1) with
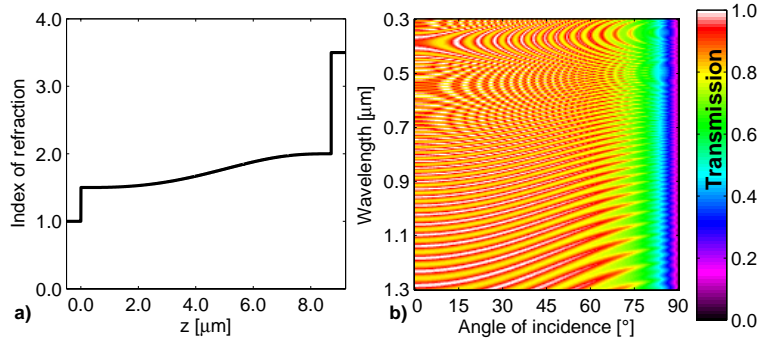
Fig. 8. a) Quintic refractive index profile and b) angle resolved transmission spectrum for limited refractive index values. The parameter n_1 was set to 1.5 and n_2 to 2.0. $\eta = 26.1\%$.

$n_1 = 1.5$ and $n_2 = 2.0$, which should be feasible using co-deposition. Figure 8 (b) shows the corresponding transmission of unpolarized light versus angle of incidence and wavelength. This transmission spectrum features Fabry-Perot-oscillations, since the interval for the refractive index is limited. For this AR-filter we calculated $\eta = 26.1\%$. In the following this value will be increased by an optimized angle and wavelength selective rugate filter, which has the same optical thickness and is limited by the same range of available refractive indices.

This small difference between 1.5 and 2.0 is not large enough for providing a broad stop band, but it is possible to increase the band width by continuously increasing the period of the refractive index profile so that the top of the coating system will reflect a different wavelength than the bottom [26]. In order to find the refractive index profile, which is optimum for these fabrication constraints, the additional constants $n_{\mathrm{min,a}}$ and $n_{\mathrm{max,a}}$ are introduced. They, respectively, represent the minimum and maximum available refractive indices. The previous formulas Eqs. (4)–(10) can still be used, but n_{inc} must be changed to $n_{\mathrm{min,a}}$, and n_{sub} to $n_{\mathrm{max,a}}$. The continuous change of the center wavelength is represented by an additional chirp parameter C, which generalizes Eq. (3) to:

$$n(t) = \sqrt{n_{\min} n_{\max}} \exp\left[\frac{\ln\left(\frac{n_{\max}}{n_{\min}}\right)}{2} \sin\left(\frac{4\pi \exp\left(\frac{Ct}{t_{\mathrm{tot}}} - \frac{C}{2}\right)}{\lambda_0} t - \frac{\pi}{2} \right) \right]. \tag{11}$$

Figure 9 (a) shows the optimized refractive index profile according to Eq. (11) and Fig. 9 (b) the corresponding angle- and wavelength dependent transmission of unpolarized light. Just like for Fig. 8, the refractive index profile was allowed to vary between 1.5 and 2.0. The optimized parameters are listed in Tab. 1. The Fabry-Perot-oscillations, which could be seen already in Fig. 8 are still present, but an efficiency of 26.9% is reached, due to the enhanced reflection around 1000 nm at oblique incidence. This solar cell efficiency corresponds to an increase of 0.8 absolute %, when compared to the AR-coating shown in Fig. 8. Due to the larger number of periods the transition between transmitting and reflecting regions in Fig. 9(b) is more sharply pronounced when compared to Fig. 7, but this comes at the expense of increased coating thickness.

In a further step we investigated the robustness of the layer systems concerning thickness errors. For this analysis we calculated the efficiencies of the optimized filters when varying the layer thicknesses, which are needed for the matrix method for calculating the filter transmission. Originally, each layer has an unmodified optical thickness of 15 nm. In each step of this analysis we varied all thicknesses, each thickness proportional to a random number, where all random numbers were distributed normally around 1.0 with individual standard deviation
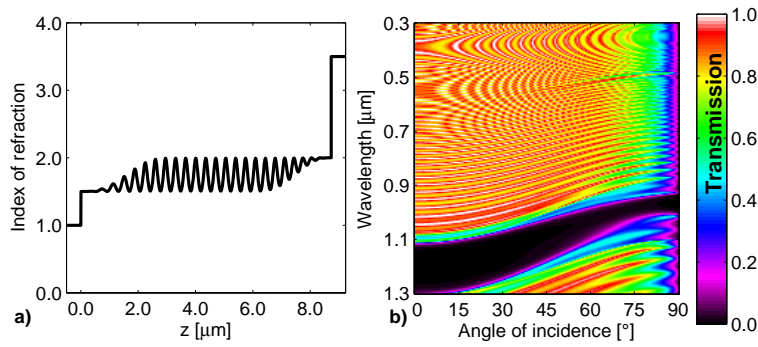
Fig. 9. a) Optimized refractive index profile and b) angle resolved transmission spectrum for limited refractive index values. $n_{\text{min,a}}$ was set to 1.5 and $n_{\text{max,a}}$ to 2.0. $\eta = 26.9\%$.

Table 1. Parameters of several filters discussed in this paper.

Figure	t_{tot} [µm]	$\frac{t_{\text{tot}}}{t_{\text{apo}}}$	A_{max}	λ_0 [µm]	C	η [%]
7	13.64	0.2739	0.9338	1.446	0.0	30.1
8	15.07		Quintic AR-coating			26.1
9	15.07	0.3252	0.9757	1.219	0.002906	26.9

σ. For each σ we performed 100 filter modifications in order to generate statistical data. The mean (solid curve) and the standard deviation corridor (dotted curve) of the calculated efficiencies are plotted in Fig. 10 for the optimized filter without refractive index limitation (a) and with limited refractive index range (b). As can be seen, the filter design is quite tolerant against fabrication errors since the cell efficiencies drop only ~ 0.1 % if each layer thickness is modified (in average) by more than 6%.
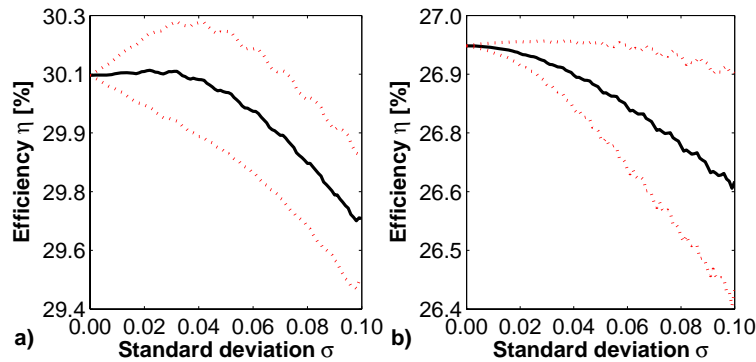

Fig. 10. Mean calculated efficiencies (solid black curve) versus relative standard deviation σ of individual layer thickness for the filter shown in (a) Fig. 7 and (b) Fig. 9. The dotted red curves represent the standard deviation corridor of 100 filter modifications.

5. Summary

We developed an analytical expression for a top coating applicable to solar cells, which decreases the transmittance of light at oblique angles of incidence close to the band gap and, thereby, increases the absorptance for normal incidence due to improved light-trapping. By neglecting absorption and dispersion in the top coating and using a realistic model for the absorbing layer, calculated efficiencies of solar cells having at least one Lambertian surface could be increased from 28.7% for a cell with zero front side reflection up to 30.1% for a solar cell equipped with the optimized angle selective filter. In order to obtain high transmission, low indices of refraction are necessary, which is at the moment a challenge for fabrication. Nevertheless, the design can be implemented on a smaller range of available refractive indices if an additional chirp parameter is included in the analytical expression. This parameter allows for a sharper transition between reflecting and transmitting behavior, at the expense of an increase in the coating thickness. This paper completely evaluates one of the first light-trapping proposals, which effectively increases photovoltaic conversion efficiencies above the limit for unconcentrated illumination.

Acknowledgements